Enhancing the Thermal Stability of Organic Solar Cells by Locking Morphology with Ethyl Cellulose Additive

Zhaochen Suo, Xiaodong Si, WenKai Zhao, Longyu Li, Jian Liu, Jie Wang, Zhaoyang Yao, Guankui Long, Chenxi Li, Xiangjian Wan,* and Yongsheng Chen*

The morphology of active layer of the organic solar cells (OSCs) tends to transition toward its lowest energy conformation under thermal stress, significantly limiting the stability of OSCs. In this study, ethyl cellulose (EC) is utilized as an additive in the active layer of the typical PM6:Y6 and other systems. Due to the strong interaction between the hydroxyl groups of EC and the heteroatoms in the organic semiconductors, their bulk heterojunction nanomorphology is locked, thereby enhancing device thermal stability. Under thermal stress at 65 °C for 1,000 h, the PM6:Y6 device incorporating EC demonstrates excellent stability nearly without performance loss. Furthermore, compared to the control device, the device exhibits improved thermal stability under a range of more stringent aging conditions. Additionally, the EC additive shows broad applicability in various active layer systems, effectively enhancing their thermal stability. This work offers a promising approach for developing stable nanomorphology structures in OSCs.

1. Introduction

Organic solar cells (OSCs), as a promising technology of clean, renewable energy, have attracted significant attention due to their advantages, including lightweight, flexibility, semitransparency, and costeffectiveness.[1] Facilitated by the rapid development of nonfullerene acceptors, OSCs have made great progress and achieved power conversion efficiencies (PCEs) around 20% in the past few years.[2] However, beyond high PCEs, the stability issue should also be addressed to realize the practical application for OSCs.[3] Generally, OSCs suffer from degradation under

thermal stress, which arises from their morphology instability primarily due to unstable phase separation of donors and acceptors during repeated heating and cooling cycles, thereby disrupting the nanoscale morphology of the active layer.[4] It is well known that an optimized nanoscale morphology in the bulk heterojunction layer is essential for OSC efficiency, as it influences charge generation, carrier transport, and collection.[5] However, this morphology represents a thermally activated metastable state that is highly sensitive to thermal aging. Over time, exposure to elevated temperatures drives the blend moves toward thermodynamic equilibrium, resulting in large-scale phase separation and a reduction in the donor–acceptor interfacial area.[6] Consequently, thermal instability remains a critical obstacle to the long-term performance of OSCs, underscoring the need for innovative strategies to maintain their morphology and enhance their durability and stability.

Several strategies have been employed to enhance the morphological stability of the active layer, which suppressed device degradation under thermal stress. For instance, many researchers have successfully utilized ternary structures to curb the tendency of large-scale crystallization and diffusion of nonfullerene acceptors (NFAs) induced by thermal stress.[7] However, this strategy demands a comprehensive component selection, and there is no universal third component applicable in different photovoltaic systems. The introduction of chemical crosslinking is another approach that can also contribute to stabilizing the morphology. Recently, Han et al. improved the thermal stability of the active layer by generating an in situ crosslinked network that forms hydrogen bonds with both the donor and acceptor, restricting their thermal motion.[8] Nevertheless, the in situ crosslinked network may require long curing times, particularly at an elevated temperature of 150 °C, to achieve its full mechanical properties. Moreover, since some insulating materials possess the inherent characteristic of high-temperature resistance or can form intermolecular interactions with the molecules of the active layer, for instance, polyacenaphthylene (PAC) can confine the motion of acceptor molecules and suppress the crystallization of acceptors at high temperatures.[9] Polyvinyl chloride (PVC) can form noncovalent interactions with conjugated donor materials.[10] Using them as additives is a simple yet effective strategy to impede thermal

Z. Suo, X. Si, L. Li, J. Liu, J. Wang, Z. Yao, C. Li, X. Wan, Y. Chen
State Key Laboratory of Elemento-Organic Chemistry
Frontiers Science Center for New Organic Matter
The Centre of Nanoscale Science and Technology and Key Laboratory of Functional Polymer Materials
Institute of Polymer Chemistry
College of Chemistry
Nankai University
Tianjin 300071, China
E-mail: xjwan@nankai.edu.cn; yschen99@nankai.edu.cn

W. K. Zhao, G. Long
School of Materials Science and Engineering
Nankai University
Tianjin 300071, China

stress-induced morphological changes. However, under the optimal proportion of polymer addition, good thermal stability and high initial efficiency of the device still cannot be concurrently obtained. For example, after adding the optimal ratio of PVC (5 wt%) in the active layer, the PCE of the device based on PM6:BO-4Cl significantly decreased from 17.3% to 15.2%.

As a commercially available cellulose derivative, EC exhibits excellent solution processability and high thermal stability.[11] Particularly, there are ≈50% remaining hydroxyl groups on EC, which offer abundant sites for hydrogen bond interactions with other groups, rendering it a good alternative as additive into organic photoactive layers. Bearing these in mind, herein, we proposed a strategy to improve the thermal stability of OSCs by incorporating EC into active layers. Using the typical PM6: Y6 system, the fresh devices with and without EC demonstrated comparable efficiencies. Under thermal stress at 65 °C for 1000 h, the device incorporating EC demonstrated exceptional stability with no observable performance degradation. Moreover, the device containing EC retained 94.5% of its initial efficiency after 270 min at 120 °C, while the control device without EC retained only 78.7% of its initial efficiency. Morphological analysis confirmed that the incorporation of EC facilitated the maintenance of optimal nanomorphology domain sizes in the active layer, primarily due to the strong interactions between hydroxyl groups on EC and heteroatoms in the active layer material. These interactions significantly enhanced the morphological stability of the active layer compared to that without the EC additive. This stable morphology mitigated the degradation of charge separation, transport, and extraction properties, thereby markedly improving thermal stability. Furthermore, the approach shows abroad applicability for enhancing the device thermal stability in other typical photovoltaic systems. The addition of EC, a solution-processable and ecofriendly stabilizer that introduces strong hydrogen bonds, represents a universal strategy for enhancing the thermal stability.

2. Results and Discussion

EC is a biodegradable and ecofriendly material synthesized through the etherification of cellulose, a natural polymer derived from renewable sources such as wood or cotton (**Figure 1**a).[12] The ethyl substitution on the cellulose backbone enhances EC's solubility and processability in common organic solvents. It is noteworthy that incomplete etherification leaves a significant amount of hydroxyl groups (≈50.5–52%) in commercially available EC. The polymer donor PM6 and the nonfullerene acceptor Y6 were selected as the model active layer system for this study (Figure 1b). The carbonyl (C=O), thiophene/benzene-F, and cyan (C≡N) groups in PM6 and Y6 could form hydrogen bonding interactions with EC. Fourier-transform infrared spectroscopy (FTIR) was used to confirm the presence of hydrogen bonding interactions between PM6, Y6, and EC. As shown in Figure 1c, the vibrational frequencies of the carbonyl groups (≈1648 cm^{-1}) and thiophene-F units (≈1364 and 1148 cm^{-1}) in PM6 shifted to lower wavenumbers in the PM6:EC blend. Similarly, the cyan groups (≈2215 cm^{-1}), carbonyl groups (≈1699 cm^{-1}), and benzene-F

units (≈1150 cm^{-1}) in Y6 exhibited blueshifts in the presence of EC.[13] To further understand the morphologies of the blend films, the Flory–Huggins interaction parameter (χ) was estimated using surface energy (γ), as given by the equation: $\chi_{DA} = (\sqrt{\gamma_D} - \sqrt{\gamma_A})^2$, where D and A represent different materials. Surface energy values of pure films were obtained from contact angle measurements (Figure 1d and Table S1, Supporting Information),[14] allowing the χ values to be calculated as 1.06, 0.91, and 0.01 for PM6:Y6, PM6:EC, and Y6:EC, respectively. Compared to PM6:Y6, the lower χ values for PM6:EC and Y6:EC suggest better miscibility of EC with these two components. Molecular dynamics (MD) simulations were conducted to further investigate the interactions between EC, PM6, and Y6 in the blend. The hydrogen bond calculations and stacking numbers of EC with PM6 and Y6 within a unit cell are presented in Figure 1e and Table S2, Supporting Information. The results indicate that EC tends to localize at the interface between PM6 and Y6, making direct contact with both materials and forming hydrogen bonds with each. These findings are consistent with the FTIR results, which help to elucidate the mechanisms through which EC stabilizes the morphology of the active layer.

To evaluate the influence of EC on the thermal stability of OSCs, inverted architecture devices consisting of indium tin oxide (ITO)/electron transport layer/PM6:Y6:EC/hole transport layer/silver (Ag) were fabricated (**Figure 2**a). To determine the optimal EC ratio for enhancing thermal stability while maintaining ideal PCE, device performance with different EC ratios was tested. Figure 2b and **Table 1** summarize the photovoltaic parameters obtained from multiple batches of devices with varying EC ratios. The control PM6:Y6 device, processed without EC, achieved a maximum PCE of 17.76%, with a short-circuit current density (J_{SC}) of 28.04 mA cm^{-2}, a fill factor (FF) of 75.05%, and an open-circuit voltage (V_{OC}) of 0.843 V, which are comparable to previously reported values.[15] Notably, incorporating EC at a low concentration does not significantly affect photovoltaic efficiency, despite EC being a high-molecular-weight insulating polymer. Consequently, the system with 0.1 mg mL^{-1} EC exhibits a PCE of 17.40%, slightly lower than that of the control device. When the EC concentration reaches 0.5 mg mL^{-1} in the CF solution, the PCE experiences a significant reduction due to a drastic decrease in V_{OC} and FF values. However, the EC devices exhibited a significant enhancement in thermal stability. After heating at 120 °C for 270 min, the PCE of the control device decreased substantially to 78.7% of its initial value. Notably, devices with various EC ratios retained >90% of their initial PCEs after accelerated aging (Figure 2c). Among these, devices with 0.1 mg mL^{-1} EC demonstrated the best thermal stability. Additionally, the addition of 0.1 mg mL^{-1} EC improved the exciton dissociation and collection properties of the devices under thermal stress, contributing to the enhancement of J_{SC} after heating (Table S4, Supporting Information). Further investigation of the photovoltaic parameters revealed that the inclusion of EC significantly enhanced the maintenance of V_{OC} and FF after heating (Figure 2d and Table S3, Supporting Information). The V_{OC} of devices with no EC, 0.05 mg mL^{-1} EC, 0.1 mg mL^{-1} EC, 0.2 mg mL^{-1} EC, and 0.5 mg mL^{-1} EC remained at 91.9, 95.1, 95.5, 95.8%,
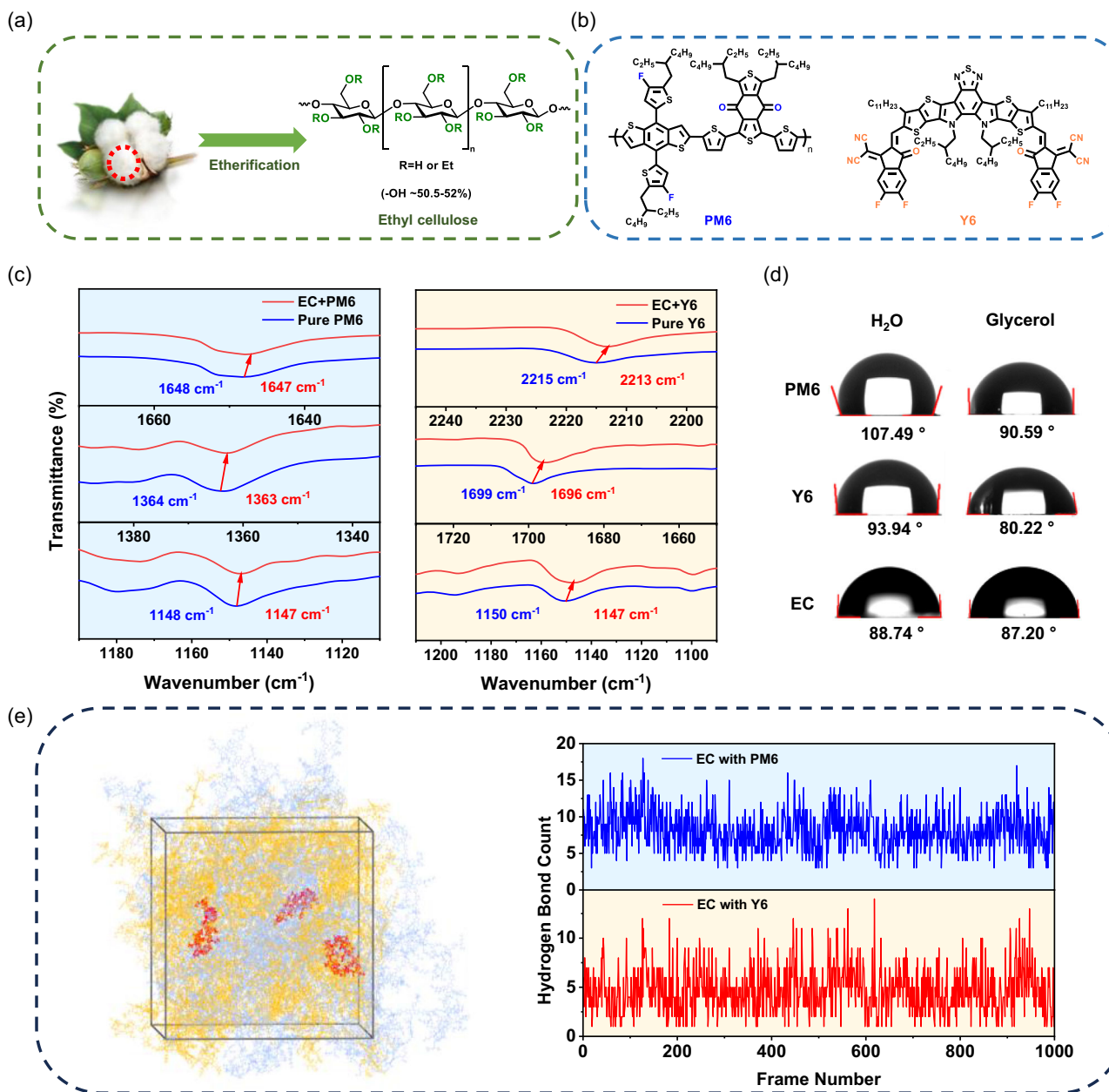
Figure 1. a) EC extracted from biomass. b) The molecular structure of PM6 and Y6. c) FTIR spectra of PM6, PM6 + EC, Y6, and Y6 + EC blends. d) Contact angles of the corresponding films. e) Snapshots of the MD simulations for the PM6:Y6:EC system: PM6 shown in blue, Y6 in orange, and EC in red. Hydrogen bonding interactions in the PM6:Y6:EC system. Herein, molecules were considered hydrogen bonded if the distance between the hydrogen atom and the H-acceptor atom was less than 2.5 Å, and the angle formed by the H-donor atom, hydrogen atom, and H-acceptor atom exceeded 90°.

and 95.5% of their original values, respectively. The FF for these devices remained at 84.0, 92.5, 94.4, 94.9, and 93.5% of their original values, respectively. These improvements are attributed to the stabilization of the nanomorphology through hydrogen bonds between EC and the active layer materials. Finally, considering both efficiencies and the results of accelerated thermal aging, 0.1 mg mL^{-1} EC was selected as the optimal additive concentration. Therefore, the standard thermal stability of control and EC-added OSCs was tested at 65 and 85 °C in the dark for ≈1000 h (Figure 2e). EC-added devices exhibited superior thermal stability compared to control devices (99.4 vs 93.7% under 65 °C and 95.3 vs 91.8% under 85 °C). It is worth noting that adding EC has no negative effect on the photostability of the device (Figure S1, Supporting Information). The photodegradation of OSC devices predominantly relies on the photochemical stability of photovoltaic materials under illumination. Herein, EC facilitates strong interactions between hydroxyl groups and heteroatoms from the organic semiconductor,
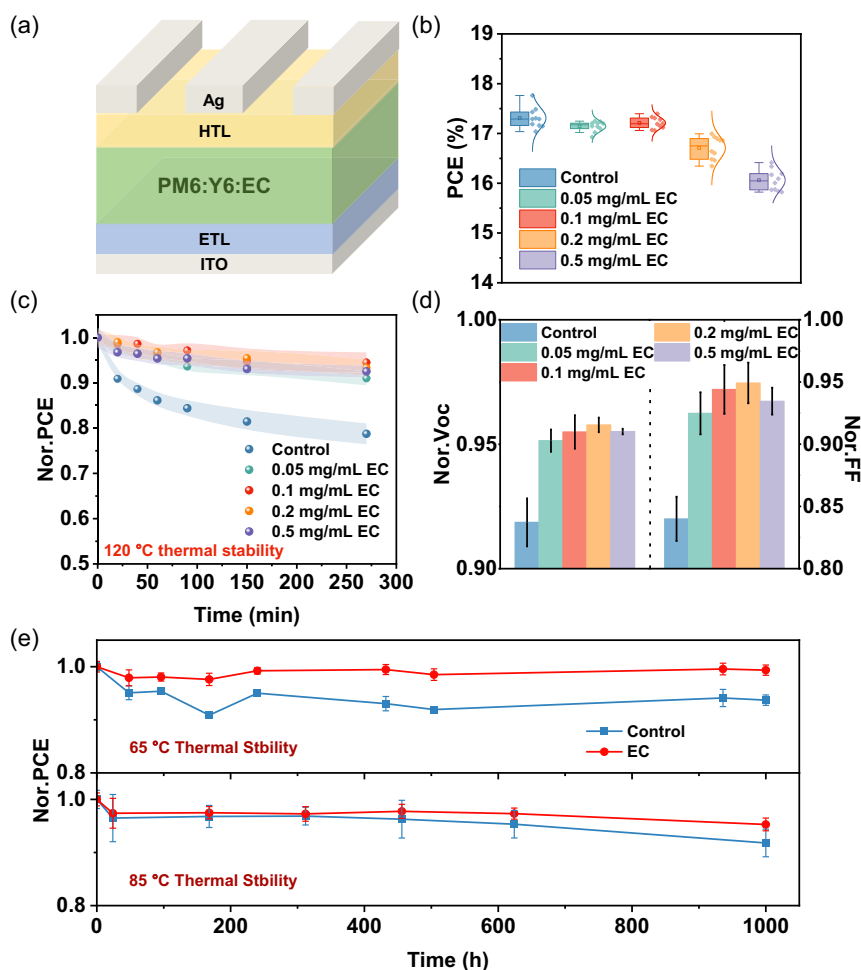
Figure 2. a) Inverted-device architecture used in this work. b) Histogram of PCEs with different ratios of EC. c) Normalized PCE of PM6:Y6 devices with different ratios of EC under the 120 °C accelerated aging process. d) Normalized V_{OC} and FF parameters of them under 120 °C accelerated aging process. e) Thermal stability test under 65 and 85 °C for control devices and devices with 0.1 mg mL^{-1} EC additive.

Table 1. Device characteristics of the OSCs based on different ratios of EC.

PM6:Y6	V_{OC} [V]	J_{SC} [mA cm^{-2}]	J_{SC}^{cal} [mA cm^{-2}]	FF [%]	PCE [%]
Control	0.843 (0.840 ± 0.002)	28.04 (27.45 ± 0.28)	26.84	75.05 (75.07 ± 0.23)	17.76 (17.31 ± 0.20)
0.05 mg mL^{-1} EC	0.839 (0.837 ± 0.003)	27.61 (27.69 ± 0.24)	–	74.58 (74.11 ± 0.26)	17.25 (17.14 ± 0.10)
0.1 mg mL^{-1} EC	0.837 (0.840 ± 0.003)	27.81 (27.25 ± 0.25)	27.04	74.42 (75.19 ± 0.53)	17.40 (17.21 ± 0.11)
0.2 mg mL^{-1} EC	0.828 (0.828 ± 0.001)	28.04 (27.90 ± 0.22)	–	73.03 (72.30 ± 0.62)	16.99 (16.71 ± 0.22)
0.5 mg mL^{-1} EC	0.826 (0.825 ± 0.002)	27.95 (27.35 ± 0.59)	–	70.99 (70.62 ± 0.56)	16.42 (15.97 ± 0.35)

effectively stabilizing nanomorphology of the bulk heterojunction layer, thus enhancing the thermal stability of devices. However, it does not inhibit the rotational dynamics of vinyl groups in Y6 or mitigate the twisting tendency within the BDT-thiophene motif.[16] Therefore, the photostability remains invariant compared to the control device.

Atomic force microscopy-infrared spectroscopy (AFM-IR) was employed to provide a more intuitive understanding of the effect of EC addition on the phase separation of the active layer. As depicted in Figure S2, Supporting Information, the root-mean-square roughness value of the EC-added blend film is 0.99 nm, which is comparable to that of the blend film without
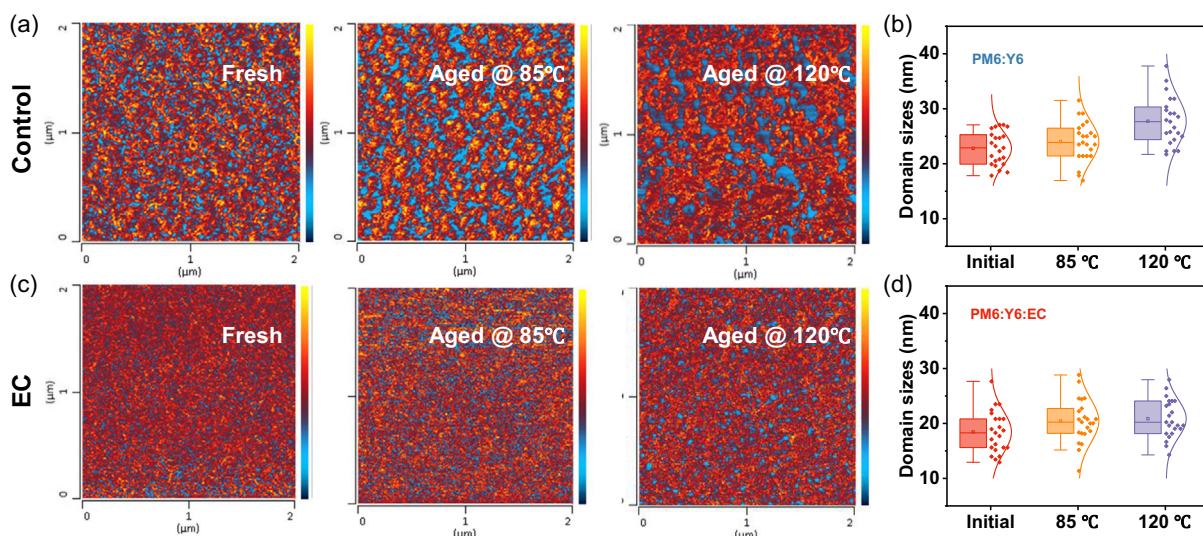
Figure 3. AFM-IR tests of a) control and c) EC-added blend films under fresh and different aging conditions. b,d) The domain sizes of these films are summarized.

EC (0.93 nm). This observation suggests that the presence of EC does not significantly alter the morphology of the original blend, which is consistent with its comparable energy conversion efficiency. We then used the characteristic absorption peak of the C≡N stretching vibration, identified in the infrared (IR) absorption spectra, to analyze the fibril structure in both control and EC-added blends, as well as in blends subjected to thermal aging (**Figure 3**a,c). Due to the unique infrared vibration signal of C≡N, which is only present in Y6, AFM-IR measurements can distinguish between the donor (PM6) and acceptor (Y6). AFM-IR spectroscopy results indicate that the average fiber size of the fresh blend film decreases slightly from 22.80 to 18.44 nm with

the addition of EC (Figure 3b,d). The primary cause for the slight reduction fiber size might be the formation of hydrogen bonds between EC and PM6 as well as Y6. However, regardless of the presence of EC, the fiber sizes remain within the widely accepted range for state-of-the-art devices (≈20 nm).[17]

After aging at 85 °C for five days and 120 °C for 270 min, the control blend film exhibited significant nanomorphological changes, including diffusion-enabled demixing and increased phase separation. Thermal stress-induced polymer reorganization and diffusion-limited aggregation of NFAs, resulting in the formation of small, isolated acceptor domains. These domains acted as morphological traps for electron transport,
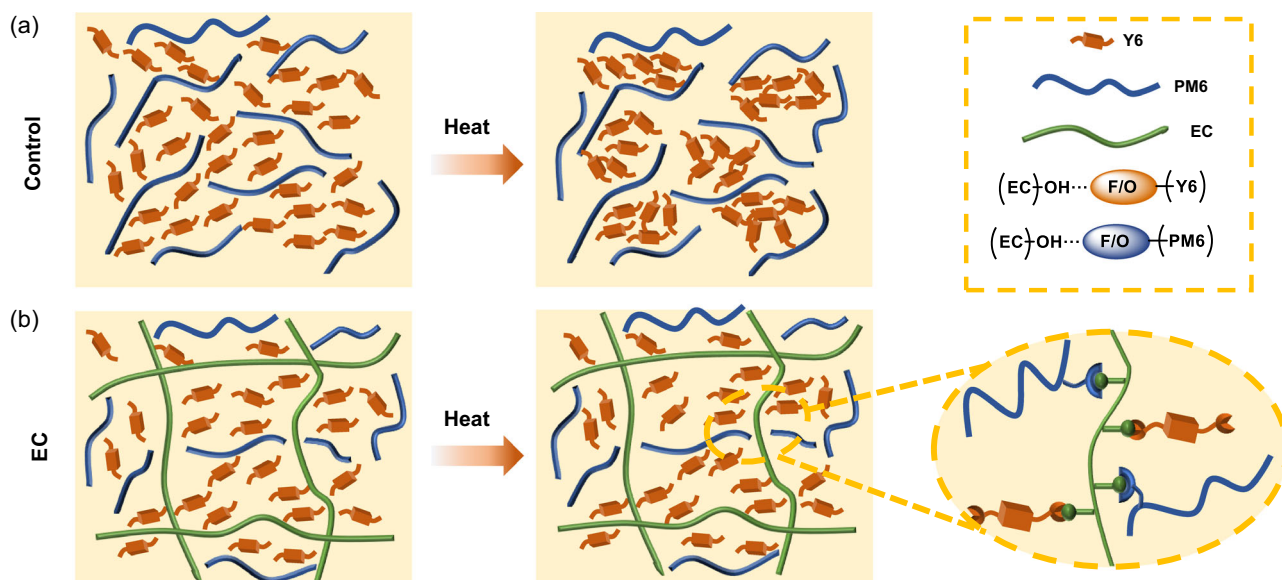
Figure 4. Morphology diagram of a) PM6:Y6 and b) PM6:Y6:EC blend films before and after aging. (F/O represents the fluorene and oxygen atoms in PM6 and Y6, which can form hydrogen bonds with hydroxyl groups in EC).
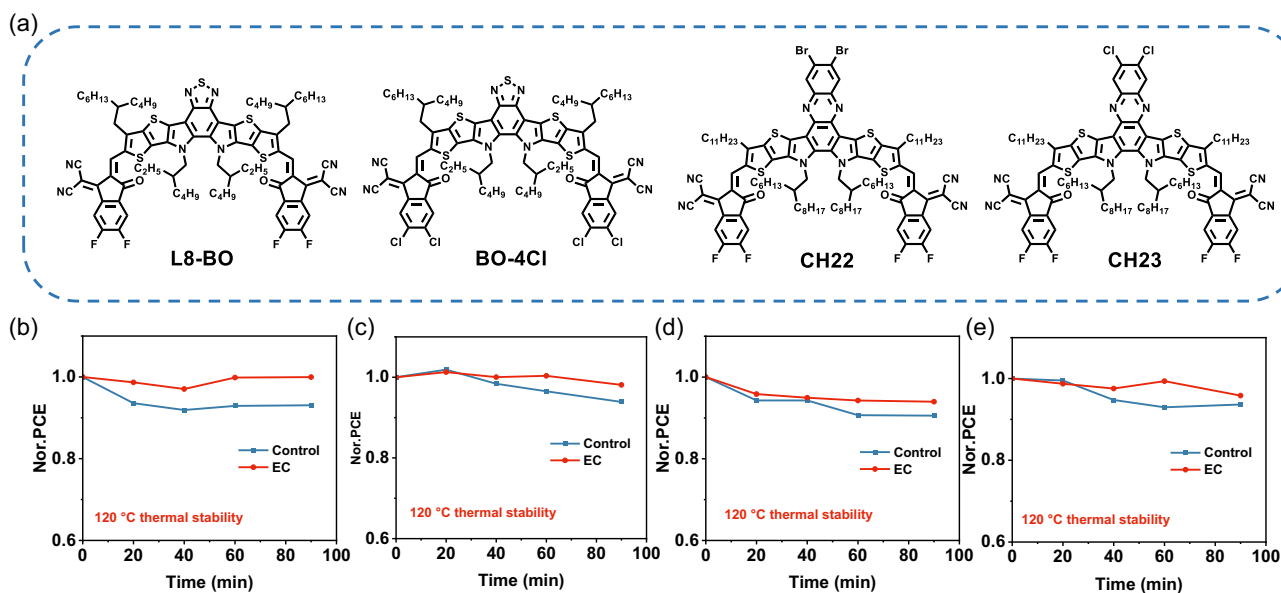
Figure 5. a) Chemical structures of L8-BO, BO-4Cl, CH22, and CH23. b–e) Thermal stability plots of the corresponding systems under 120 °C with and without EC.

leading to long-term FF degradation.[6] The dark J–V measurements correlate well with the AFM-IR results (Figure S3, Supporting Information). In contrast, the addition of EC, which features hydrogen bonding interactions, effectively preserved the nanomorphology. Under identical aging conditions, EC acted as a stabilizer, maintaining the initial nanomorphology of the active layer blend. Line profiles of AFM-IR images are shown in Figure S4, Supporting Information, where the full width at half maximum of the peaks was used to estimate the fibril width. Following heating at 85 °C for 5 days and aging at 120 °C for 270 min, the average fibril width of the control blend increased from 22.80 to 24.04 and 27.74 nm, respectively. However, in the EC-added system, the average values remained at 20.45 and 20.86 nm, respectively, demonstrating the significant role of EC in stabilizing the morphology and enhancing the thermal stability of OSCs.

Figure 4a illustrates that the photoactive layer of OSCs exists in a thermodynamically metastable state, which transitions to a higher entropic energy under thermal stress, resulting in increased acceptor aggregation and reduced photovoltaic performance. In contrast, in the PM6:Y6:EC film, the hydroxyl groups in EC form non-covalent interactions with the heteroatoms, such as F or O, in both PM6 and Y6, thereby restricting the diffusion of PM6 and Y6 molecules and preventing phase separation induced by thermal stress, as shown in Figure 4b. This interaction ultimately enhances thermal stability.

As established through the aforementioned systematic investigations, ecofriendly EC serves as an effective stabilizer for enhancing the thermal stability of organic photovoltaics. To assess the general applicability of EC, a variety of more efficient acceptors, including L8-BO, BO-4Cl, CH22, and CH23, were employed in device fabrication (**Figure 5a**).[2d,18] Notably, PCEs of these four photovoltaic systems remained nearly unaffected by the incorporation of 0.1 mg mL^{-1} EC, as illustrated in

Table S5, Supporting Information. The addition of EC significantly enhances the thermal stability of these devices, as demonstrated in Figure 5b–e. After exposure to 120 °C for 90 min, the PCEs of devices with EC based on PM6:L8-BO, PM6:BO-4Cl, PM6:CH22, and PM6:CH23 remained at 99.9, 98.1, 94.0, and 95.8% of their original efficiencies, respectively. In contrast, the PCEs exhibited reductions to 93.1, 93.9, 90.6, and 93.6% compared to their initial efficiencies, respectively. These results further highlight the broad applicability and effectiveness of the EC additive strategy.

3. Conclusion

In conclusion, we have proposed a strategy to significantly enhance the thermal stability of OSCs by the incorporation of an additive EC into active layers. EC can serve as a stabilizer in bulk heterojunction layers to freeze the nanomorphology due to strong interaction between hydroxyl groups on EC and the heteroatoms in organic active layer materials. The EC-based OSC devices can withstand at 65 °C for 1000 h without apparently losing performance and maintain stability under more stringent conditions. Importantly, the EC additive has no negative effect on the device's photostability. Furthermore, this environment-friendly EC additive demonstrated broad applicability for other representative photovoltaic material systems. Our findings present an effective strategy via intramolecular interaction to freeze active layer morphology, thereby enhancing the thermal stability of OSCs.

Supporting Information

Supporting Information is available from the Wiley Online Library or from the author.

Conflict of Interest

The authors declare no conflict of interest.

Author Contributions

Zhaochen Suo: conceptualization (lead); data curation (lead); investigation (equal); writing—original draft (lead). **Xiaodong Si**: investigation (equal); methodology (equal). **WenKai Zhao**: data curation (supporting); methodology (supporting); software (lead). **Longyu Li**: data curation (supporting); methodology (supporting); visualization (supporting); writing—original draft (supporting). **Jian Liu**: data curation (supporting); resources (supporting). **Jie Wang**: data curation (supporting); resources (supporting). **Zhaoyang Yao**: investigation (supporting). **Guankui Long**: data curation (lead); methodology (lead); software (lead). **Chenxi Li**: conceptualization (lead); investigation (lead). **Xiangjian Wan**: conceptualization (lead); funding acquisition (lead); project administration (lead); supervision (lead); writing—review & editing (lead). **Yongsheng Chen**: conceptualization (lead); funding acquisition (lead); project administration (lead); resources (lead); supervision (lead); writing—review & editing (lead). **Zhaochen Suo** and **Xiaodong Si** contributed equally to this work.

Data Availability Statement

The data that support the findings of this study are available in the supplementary material of this article.

[1] a) X. Zheng, L. Zuo, K. Yan, S. Shan, T. Chen, G. Ding, B. Xu, X. Yang, J. Hou, M. Shi, H. Chen, *Energy Environ. Sci.* **2023**, *16*, 2284; b) Z. Xiao, J. Liu, X. Chen, Z. Suo, X. Cao, N. Xu, Z. Yao, C. Li, X. Wan, Y. Chen, *J. Mater. Chem. A* **2025**, 13, 2301–2308; c) H. Li, J. Le, H. Tan, L. Hu, X. Li, K. Zhang, S. Zeng, Q. Liu, M. Zhang, L. Shi, Z. Cai, S. Liu, H. Li, L. Ye, X. Hu, Y. Chen, *Adv. Mater.* **2024**, 2411989, https://doi.org/10.1002/adma.202411989; d) D. Wang, H. Liu, Y. Li, G. Zhou, L. Zhan, H. Zhu, X. Lu, H. Chen, C.-Z. Li, *Joule* **2021**, *5*, 945; e) S. Feroze, A. Distler, L. Dong, M. Wagner, I. A. Channa, F. Hoga, C. J. Brabec, H.-J. Egelhaaf, *Energy Environ. Sci.* **2025**, 18, 674–688.

[2] a) Y. H. Liu, B. W. Li, C. Q. Ma, F. Huang, G. T. Feng, H. Z. Chen, J. H. Hou, L. P. Yan, Q. Y. Wei, Q. Luo, Q. Y. Bao, W. Ma, W. Liu, W. W. Li, X. J. Wan, X. T. Hu, Y. C. Han, Y. W. Li, Y. H. Zhou, Y. P. Zou, Y. W. Chen, Y. F. Li, Y. S. Chen, Z. Tang, Z. C. Hu, Z. G. Zhang, Z. S. Bo, *Sci. China Chem.* **2022**, *65*, 224; b) X. J. Wan, C. X. Li, M. T. Zhang, Y. S. Chen, *Chem. Soc. Rev.* **2020**, *49*, 2828; c) J. Yuan, Y. Q. Zhang, L. Y. Zhou, G. C. Zhang, H. L. Yip,
T. K. Lau, X. H. Lu, C. Zhu, H. J. Peng, P. A. Johnson, M. Leclerc, Y. Cao, J. Ulanski, Y. F. Li, Y. P. Zou, *Joule* **2019**, *3*, 1140; d) C. Li, J. D. Zhou, J. L. Song, J. Q. Xu, H. T. Zhang, X. N. Zhang, J. Guo, L. Zhu, D. H. Wei, G. C. Han, J. Min, Y. Zhang, Z. Q. Xie, Y. P. Yi, H. Yan, F. Gao, F. Liu, Y. M. Sun, *Nat. Energy* **2021**, *6*, 605; e) L. Zhu, M. Zhang, J. Q. Xu, C. Li, J. Yan, G. Q. Zhou, W. K. Zhong, T. Y. Hao, J. L. Song, X. N. Xue, Z. C. Zhou, R. Zeng, H. M. Zhu, C. C. Chen, R. C. I. MacKenzie, Y. C. Zou, J. Nelson, Y. M. Zhang, Y. M. Sun, F. Liu, *Nat. Mater.* **2022**, *21*, 656; f) Y. Jiang, S. Sun, R. Xu, F. Liu, X. Miao, G. Ran, K. Liu, Y. Yi, W. Zhang, X. Zhu, *Nat. Energy* **2024**, *9*, 975; g) C. Chen, L. Wang, W. Xia, K. Qiu, C. Guo, Z. Gan, J. Zhou, Y. Sun, D. Liu, W. Li, T. Wang, *Nat. Commun.* **2024**, *15*, 6865; h) L. Zhu, M. Zhang, G. Zhou, Z. Wang, W. Zhong, J. Zhuang, Z. Zhou, X. Gao, L. Kan, B. Hao, F. Han, R. Zeng, X. Xue, S. Xu, H. Jing, B. Xiao, H. Zhu, Y. Zhang, F. Liu, *Joule* **2024**, *8*, 3153; i) Z. Yao, X. Wan, C. Li, Y. Chen, *Acc. Mater. Res.* **2023**, *4*, 772; j) X. Li, X. Kong, G. Sun, Y. Li, *eScience* **2023**, *3*, 100171.

[3] Q. Burlingame, M. Ball, Y.-L. Loo, *Nat. Energy* **2020**, *5*, 947.

[4] a) Y. Qin, N. Balar, Z. Peng, A. Gadisa, I. Angunawela, A. Bagui, S. Kashani, J. Hou, H. Ade, *Joule* **2021**, *5*, 2129; b) S. Alam, H. Aldosari, C. E. Petoukhoff, T. Váry, W. Althobaiti, M. Alqurashi, H. Tang, J. I. Khan, V. Nádaždy, P. Müller-Buschbaum, G. C. Welch, F. Laquai, *Adv. Funct. Mater.* **2023**, *34*, 2308076; c) M. Li, L. Tian, F. He, *Aggregate* **2024**, *5*, e567.

[5] a) X. Zhou, W. Liang, R. Ma, C. Zhang, Z. Peng, T. A. P. Dela Peña, J. Wu, Z. Ma, Y. Liao, G. Li, H. Hu, *Energy Environ. Sci.* **2024**, *17*, 7762; b) N. Wei, J. Chen, Y. Cheng, Z. Bian, W. Liu, H. Song, Y. Guo, W. Zhang, Y. Liu, H. Lu, J. Zhou, Z. Bo, *Adv. Mater.* **2024**, *36*, 2408934; c) R. Lin, H. Zhou, X. Xu, X. Ouyang, *Dyes Pigm.* **2024**, *224*, 111980.

[6] X. Du, T. Heumueller, W. Gruber, O. Almora, A. Classen, J. Qu, F. He, T. Unruh, N. Li, C. J. Brabec, *Adv. Mater.* **2020**, *32*, 1908305.

[7] a) W. Y. Yang, Z. H. Luo, R. Sun, J. Guo, T. Wang, Y. Wu, W. Wang, J. Guo, Q. Wu, M. M. Shi, H. N. Li, C. L. Yang, J. Min, *Nat. Commun.* **2020**, *11*, 1218; b) C. Zhang, M. Zhang, Q. Zhou, S. Chen, S. Kim, J. Yao, Z. Zhang, Y. Bai, Q. Chen, B. Chang, H. Fu, L. Xue, H. Wang, C. Yang, Z. G. Zhang, *Adv. Funct. Mater.* **2023**, *33*, 2214392; c) Y. Wang, H. Gao, M. Sun, C. T. Lin, H. Li, F. R. Lin, B. Fan, Z. Li, J. A. Zapien, A. K. Y. Jen, *Adv. Energy Mater.* **2024**, *14*, 2304449.

[8] J. Han, H. Xu, A. Sharma, M. Babics, J. Bertrandie, X. Wang, L. Huerta Hernandez, Y. Zhang, Y. Wen, D. Rosas Villalva, N. Ramos, S. H. K. Paleti, J. Martin, F. Xu, J. Troughton, R. Yang, J. Gorenflot, F. Laquai, S. De Wolf, D. Baran, *Joule* **2024**, *8*, 2883.

[9] F. Chen, Y. Zhang, Q. Wang, M. Gao, N. Kirby, Z. Peng, Y. Deng, M. Li, L. Ye, *Chin. J. Chem.* **2021**, *39*, 2570.

[10] C. Guan, C. Xiao, X. Liu, Z. Hu, R. Wang, C. Wang, C. Xie, Z. Cai, W. Li, *Angew. Chem., Int. Ed.* **2023**, *62*, e202312357.

[11] D. Yang, X. Peng, L. Zhong, X. Cao, Y. Chen, X. Zhang, S. Liu, R. Sun, *Carbohydr. Polym.* **2014**, *103*, 198.

[12] J. Y. Wu, Y. J. Liu, A. Islam, Q. H. Zheng, J. G. Li, W. Ji, L. H. Chen, X. H. Ouyang, *Adv. Sci.* **2020**, *7*, 1902269.

[13] J. Zhang, Q. Chen, M. Li, G. Zhang, Z. Zhang, X. Deng, J. Xue, C. Zhao, C. Xiao, W. Ma, W. Li, *Adv. Mater.* **2024**, *36*, 2312805.

[14] a) J. Comyn, *Int. J. Adhes. Adhes.* **1992**, *12*, 145; b) S. Nilsson, A. Bernasik, A. Budkowski, E. Moons, *Macromolecules* **2007**, *40*, 8291.

[15] Z. Suo, Z. Xiao, S. Li, J. Liu, Y. Xin, L. Meng, H. Liang, B. Kan, Z. Yao, C. Li, X. Wan, Y. Chen, *Nano Energy* **2023**, *118*, 109032.

[16] J. Han, H. Xu, S. H. K. Paleti, A. Sharma, D. Baran, *Chem. Soc. Rev.* **2024**, *53*, 7426.

[17] a) Y. H. Liu, B. W. Liu, C. Q. Ma, F. Huang, G. T. Feng, H. Z. Chen, J. H. Hou, L. P. Yan, Q. Y. Wei, Q. Luo, Q. Y. Bao, W. Ma, W. Liu, W. W. Li, X. J. Wan, X. T. Hu, Y. C. Han, Y. W. Li, Y. H. Zhou, Y. P. Zou,

Y. W. Chen, Y. Q. Liu, L. Meng, Y. F. Li, Y. S. Chen, Z. Tang, Z. C. Hu, Z. G. Zhang, Z. S. Bo, *Sci. China Chem.* **2022**, *65*, 1457; b) M. Zhang, L. Zhu, T. Hao, G. Zhou, C. Qiu, Z. Zhao, N. Hartmann, B. Xiao, Y. Zou, W. Feng, H. Zhu, M. Zhang, Y. Zhang, Y. Li, T. P. Russell, F. Liu, *Adv. Mater.* **2021**, *33*, 2007177; c) Y. Cai, Q. Li, G. Lu, H. S. Ryu, Y. Li, H. Jin, Z. Chen, Z. Tang, G. Lu, X. Hao, H. Y. Woo, C. Zhang, Y. Sun, *Nat. Commun.* **2022**, *13*, 2369; d) L. Zhu, M. Zhang, J. Xu, C. Li, J. Yan, G. Zhou, W. Zhong, T. Hao, J. Song, X. Xue, Z. Zhou, R. Zeng, H. Zhu, C.-C. Chen, R. C. I. MacKenzie, Y. Zou, J. Nelson, Y. Zhang, Y. Sun, F. Liu, *Nat. Mater.* **2022**, *21*, 656; e) J. Zhou, L. Wang, C. Liu, C. Guo, C. Chen, Y. Sun, Y. Yang, J. Cheng, Z. Gan, Z. Chen, W. Sun, J. Zhou, W. Xia, D. Liu, W. Li, T. Wang, *J. Am. Chem. Soc.* **2024**, *146*, 34998.

[18] a) Y. Cui, H. Yao, L. Hong, T. Zhang, Y. Tang, B. Lin, K. Xian, B. Gao, C. An, P. Bi, W. Ma, J. Hou, *Natl. Sci. Rev.* **2020**, *7*, 1239; b) H. Liang, H. Chen, P. Wang, Y. Zhu, Y. Zhang, W. Feng, K. Ma, Y. Lin, Z. Ma, G. Long, C. Li, B. Kan, Z. Yao, H. Zhang, X. Wan, Y. Chen, *Adv. Funct. Mater.* **2023**, *33*, 2301573; c) H. Liang, X. Bi, H. Chen, T. He, Y. Lin, Y. Zhang, K. Ma, W. Feng, Z. Ma, G. Long, C. Li, B. Kan, H. Zhang, O. A. Rakitin, X. Wan, Z. Yao, Y. Chen, *Nat. Commun.* **2023**, *14*, 4707.